ISAV

Journal of Theoretical and Applied Vibration and Acoustics

journal homepage: http://tava.isav.ir

Design and Fabrication of Low-Frequency Inductive Velocity Transducer for Condition Monitoring of Large-Scale Steam Turbines

Alireza Alavi, Ali Chaibakhsh *

[i.] *Faculty of Mechanical Engineering, University of Guilan, Rasht, Iran*
[ii.] *Intelligent Systems and Advanced Control Lab, University of Guilan, Rasht, Iran*

ARTICLE INFO

Receive Date:
Revise Date:
Accept Date:

Keywords:
Vibration Measurement
Electromagnetic
Induction Sensor
Velocity Transducer
Condition Monitoring
Rotating Machinery

ABSTRACT

Vibration sensors are key equipment in monitoring the condition and performance of rotating systems, especially in sensitive industries such as oil and gas and power plants. In rotating systems with high moment of inertia, such as large steam and gas turbines, due to the low frequency range of vibrations, the use of speed transducers with appropriate sensitivity is essential. This study is dedicated to the design, simulation, and construction of a single-coil vibration sensor, which was developed with the aim of achieving a sensitivity of 10 mV/mm/s. The various components of the transducer, including the permanent magnet, coil, flat springs, and housing, were designed and fabricated using a reverse-engineering approach supported by detailed analysis of an existing commercial sensor. To determine the material and physical characteristics of the parts, experimental tests and field measurements were used, and modeling based on the law of electromagnetic induction was carried out to analyze the behavior of the sensor. Experimental results show that the produced sensor has an entirely linear voltage-velocity behavior with a sensitivity slope of 9.4374 mV/mm/s, which can be accurately compensated using a calibrated transmitter circuit. The operation of this sensor in the frequency range of 3 to 1200 Hz makes it a suitable option for use in heavy industrial conditions.

doi: ***

*Corresponding author: Ali Chaibakhsh
Email address: chaibakhsh@guilan.ac.ir

1- Introduction

Monitoring rotating machinery and equipment, such as gas and steam turbines, is critically important due to substantial costs of repairs, production downtime and maintenance [1, 2]. Uncontrolled vibrations in such machines can lead to severe consequences including excessive noise, misalignments and amplified oscillations, unwanted load increases on bearing, accelerated wear and damage of components, and finally, a significant reduction in the operational lifetime of the equipment [3, 4].

Fault diagnosis of rotating machinery based on data-driven approaches, utilizing information acquired from vibrometric sensors and subsequent vibration behavior analysis, is widely recognized as an effective strategy for enhancing system reliability, operational safety, and service life [5, 6]. However, the effectiveness of such approaches is strongly dependent on the quality, measurement accuracy, and reliability of the sensors employed. This dependency highlights the critical importance of developing robust and accurate measurement instrumentation, along with the application of reliable signal processing and analysis techniques [7].

Vibrometric sensors / transducers are electromechanical velocity measurement equipment that play a key role in the dynamic monitoring of rotating machines. Their performance is particularly crucial in vibration analysis of complicated systems, which made them one of the widely used sensors for fault detection and diagnosis in industrial machinery [8, 9]. Structural or mechanical defects in a dynamic system inevitably alter their vibration characteristics, affecting not only the amplitude but also the frequency spectrum of the subsequent vibrational signals [10]. Therefore, precise analysis of vibration signals can provide valuable insights into the health and performance of rotating components [11].

Under special operating conditions, such as high temperatures or very low frequency vibrations, commonly encountered in large-scale systems such as steam turbines, using speed-based vibrometric sensors becomes essential for accurate condition monitoring [8, 12]. Numerous companies and researchers have been focused on developing vibrometers with higher accuracy, improved linearity, and less sensitivity to noise by enhancing the structure, materials and components. In response to the technical challenges in developing such sensors, significant improvements have been made in the performance of inductive speed sensors. The main focuses of these studies have been the optimization of magnetic materials and the internal sensor structure with the aim to increase sensitivity and improve the signal-to-noise ratio (SNR) [13]. Many innovative designs in the structure and geometric arrangement of the sensors have been performed to improve the performances of vibrometric sensor. Coil winding technologies, which play a fundamental role in the construction of sensors, can be very complex and originate in different structures, including single or multiple coils, or wound in one or more layers [14]. These coils are widely used in actuators such as electromagnets and electric motors, as well as in moving coil systems, sensors, and various precision measuring devices [15].

Another major technical challenge in designing the magnetic field structure of these sensors is the limited magnetic field strength and non-uniform distribution within the active air gap. These issues are primarily caused by using of axially magnetized permanent magnets and magnetic boots mounted on both ends of the permanent magnet [16]. Yao et al. innovatively proposed a dual magnetic ring magnetic field structure to solve this problem. This structure uses concentric and radially-magnetized ring-shaped permanent magnets in combination with adaptive ring-shaped magnetic boots. This combination, using an embedded yoke, creates an efficient closed magnetic circuit, so that the magnetic flux density is increased by 146.67% [17]. Zhou et al., using a concentric bi-magnet structure, succeeded in optimizing the magnetic field distribution and increased the sensitivity of the inductive speed sensor by about 24% without increasing the magnet volume [16]. In their study, Hong et al. introduced a closed magnetic field structure that, by creating a more uniform magnetic field distribution and higher output voltage in the coil, increased the magnetic field intensity by 24% compared to the conventional semi-closed configuration [18]. As well. Huang et al. (2022) designed a two-coil micro-impedance resonance sensor for online detection and impurity analysis of mechanical lubrication systems. With this work, the detection sensitivity of the sensor was improved [19]. Mirzaei et al (2020), presented an eddy current velocity sensor with ferromagnetic shielding. The design consists of aluminum or hard iron-based moving parts, an excitation coil and two coupling coils covered by a thin steel layer. This compact and simple structure offers excellent linearity in various magnetic materials, while the shielding increases sensitivity and minimizes interference from nearby ferromagnetic objects [20].

This study aims to design and fabricate a single-coil inductive velocity transducer for vibration measurement in high moment-of-inertia rotating machinery, such as power plant steam turbines. In such systems, due to their large mass and slow dynamic response, a vibration sensor with minimal mechanical complexity is required to ensure accurate, reliable, and stable signal acquisition. Accordingly, the designed sensor is optimized to provide a stable and linear response in the frequency range of 10 to 1200 Hz, which perfectly aligns with the typical vibration spectrum of large-scale rotating machinery. The sensor is expected to accurately and linearly measure vibration velocity in this range, without requiring any external power supply, while maintaining low sensitivity to noise.

It should be noted that the contribution of this study does not lie in introducing a novel sensor topology. Rather, the main contribution resides in the systematic reverse-engineering-based development of a low-frequency inductive velocity transducer, supported by detailed fabrication procedures and experimental optimization of key mechanical components, particularly the flat suspension springs. The presented methodology bridges the gap between existing commercial sensor concepts and reproducible laboratory-scale fabrication, and is validated through experimental testing for condition monitoring of large-scale steam turbines.

The rest of the paper is organized as follows: Section 2 presents the description and operating principle of the sensor. Section 3 details the mechanical design and fabrication process. Section 4 focuses on experimental tests and accuracy verification of the sensor. Finally, Section 5 provides conclusions and suggestions for future research.

2- Sensor Description and Operating Principle

Velocity transformers or vibrometer sensors are a type of electromechanical sensor used to monitor relatively large rotating equipment such as turbines, pumps, motors, and compressors, especially in cases where measuring vibration velocity is preferred over acceleration or displacement, and are used to directly measure vibrational motion [21].

In Figure 1, a schematic of a vibrometer sensor is shown. The internal structure of vibrometery sensors consists of three main components: a permanent magnet that produces a constant magnetic field, a single stationary coil located inside the sensor housing, axially overlapping the moving permanent magnet, and finally a spring suspension system that allows the magnetic core to move independently. As vibration occurs, the relative motion between coil and magnet produces an induced voltage, according to Faraday's law, which is proportional to the relative speed of vibration.

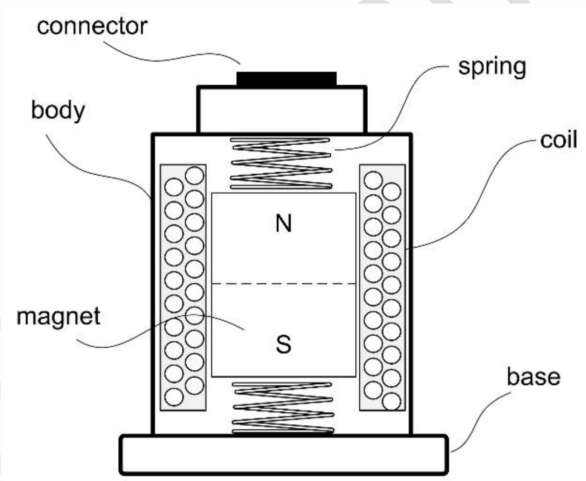

Figure 1. Schematic of single-coil winding vibrometer transducer

Key advantages of this type of sensor include no need for an external power supply and nearly constant and linear sensitivity over a specific frequency range, usually between 10 Hz and 1000 Hz [3]. Compared to dual-coil designs, single-coil vibration sensors benefit from a simpler mechanical structure and circuit, which consequently reduces their size, weight, and manufacturing costs. These characteristics make single-coil sensors a more suitable and cost-effective option in applications that are not exposed to severe noise or where very high precision is not required [13]. In Table 1, the main features of single-coil vibrometer sensor in comparison with dual coil sensors are presented.

Table 1. Features of a single-coil winding vibrometer sensor

Feature	Single-Coil Winding	Dual-Coil Winding
Design simplicity	Higher	More complex
Size and weight	Smaller	Larger
Sensitivity to motion direction	Maybe directional	Better in both directions
Output signal strength	Maybe weaker	Stronger and more stable
Noise susceptibility	Potentially higher	Reduced via differential design
Cost and manufacturing	More economical	More expensive

In Table 2, the summary of the design requirements and solutions for the vibrometer sensor are presented. In a single-coil velocity transducer, the governing equations are derived from fundamental electromagnetic principles, particularly Faraday's law of induction, as well as basic electrical circuit relationships. These relations form the basis for modeling the sensor's behavior and characterizing its response to vibrational motion [22].

Faraday's law of induction (production of e.m.f. due to changing magnetic flux)

$$\frac{d\Phi(t)}{dt}e(t) = -N \qquad (1)$$

$e(t)$: Induced electromotive force (V)

N : The number of wire loops around the coil

Φ: Magnetic flux (Wb)

in which, Φ(t) is the magnetic flux through the coil, is given by:

$$\Phi(t) = B(t)A\cos(\theta) \qquad (2)$$

$B(t)$:Magnetic flux density (T)

A : The cross section of the coil (m^2)

θ: Flux angle and line perpendicular to the surface (rad)

The induced e.m.f. can be calculated according to the relative velocity between the coil and the constant magnetic field B as follows,

$$e(t) = N.B.l.v(t) \qquad (3)$$

l :Effective length of the coil (m)

$v(t)$: Relative velocity (m/s)

By considering inductance (as an RL circuit), we have [23],

$$V(t) = L\frac{d\,i(t)}{dt} + R\,.\,i(t) \tag{4}$$

$i(t)$: Induced current (A)

R: Coil resistance (Ω)

L: Coil inductance (H)

$V(t)$: Thermical voltage (V)

In addition, the inductance of the coil can be written approximately as,

$$L = \mu_0 \frac{N^2.A}{l} \tag{5}$$

μ_0: Vacuum permeability ($4\pi\times10^{-7}$ H/m)

And finally, the coil factor k can be obtained as,

$$k = N \cdot B \cdot l \quad \text{hence,} \quad e(t) = k\,v(t) \tag{6}$$

Based on the relationships between the induced voltage and current with the magnetic flux density and the time-varying magnetic flux, both the induced e.m.f. and the current in the coil can be calculated and simulated. In this analysis, it is assumed that the magnetic flux is aligned with the vector perpendicular to the coil surface ($\theta = 0$). The core permeability is taken to be one due to the absence of a ferromagnetic core in the coil structure. Due to the small dimensions of the coil (axial length of only 25 mm), the allowable stroke of the moving magnetic core is significantly limited. As a result, the achievable sensitivity is inherently limited. Accordingly, the sensitivity coefficient of the coil k is conservatively assumed to be 10 *(mV/mm)*, and all subsequent calculations and simulations are performed based on this value.

Table 2. Vibrometer sensor design requirements and corresponding solutions

Design Requirements	Technical Function	Effects on output	Solution
Single-coil winding	Enables a compact and cost-effective sensor structure.	More susceptible to environmental noise and directional sensitivity.	Compensated by increasing magnetic flux density (B) and / or number of turns (N).
High magnetic flux (B)	Provides a strong and stable magnetic field across the coil.	Increases induced voltage (e.m.f.) even with small displacements.	Use of neodymium magnets with optimized geometry.
Large number of turns (N)	Enhances total induced e.m.f. linearly concerning to vibration velocity.	Improves output sensitivity significantly.	Use a thin wire (thinner than 50 μm) to allow a high number of turns (more than 10,000) within limited spaces.
Small sensor dimensions	Ensures compact integration in industrial systems with space limitations.	Limits the stroke/displacement of the moving core.	Optimize magnetic circuit and maximize flux linkage per mm of displacement.

Moving magnetic core	Creates time-varying magnetic flux through the stationary coil.	Maintains strong coupling; improves e.m.f. generation efficiency.	Use a balanced axial guidance system for smooth core motion during vibration.

3- Mechanical Design and Fabrication Process

Designing and fabricating a reliable and accurate vibrometer sensor requires not only a thorough understanding of its operating principles and detailed knowledge of the mechanical and electromagnetic behavior of each component, but also careful selection of materials and manufacturing processes. Achieving optimal performance requires an integrated approach that adeptly balances precision engineering and the practical constraints in fabrication.

In this study, given the availability of a reference industrial sensor, the design approach was based on re-engineering the functional and structural details of the existing sample. Since it was not possible to precisely calculate certain dynamic parameters, such as the natural frequency of internal elements or exact electromagnetic coupling behaviors, the mechanical design was approached by emphasizing on the material similarity and mechanical compatibility with the reference model. This strategy ensured that the correct functioning of the final sensor was maintained at an acceptable level.

The material identification process began with a visual and qualitative analysis of each component based on appearance, weight, magnetic, and conductive properties. The final material of the components was then confirmed using simple tests such as density measurement, electrical conductivity, and magnetic testing. By identifying the materials and appropriate manufacturing process, each method was selected by compromising between precision, cost-effectiveness, and local availability.

3.1. Electromagnetic Design

The design process started from the innermost component of the sensor. The moving permanent magnet governs the generated e.m.f. and defines the geometrical limitation and dimensions of surrounding components. By examining different neodymium magnet grades, the best match to the reference sample was selected in terms of dimensions and magnetic power. The field strength at the center of cylindrical neodymium magnets of various grades and dimensions was investigated, and all possible cases were calculated using the K&J Magnetics calculator [24]. In Figure 2, the magnetic field calculation results for NdFeB grade N42 are presented.

The design process was carried out by solving the governing electromagnetic equations in the Maplesoft™ environment to predict the expected sensor sensitivity. The model incorporated key design and operating parameters, including an axial magnetic flux density of $B \approx 0.54$ T, obtained from Fig. 2 for the selected N42 NdFeB permanent magnet at the coil center. A sinusoidal vibration velocity with a peak amplitude of 5 mm/s was assumed, representing typical operating conditions in large-scale rotating machinery. The geometric parameters of the coil were defined as an inner diameter of 20 mm, a wire diameter of 50 µm, and an axial length of 25 mm, selected to balance sensitivity, manufacturability, and spatial constraints. Based on these inputs, the model enabled estimation of the induced electromotive force and sensitivity. The detailed specifications of the selected neodymium magnet are summarized in Table 3.

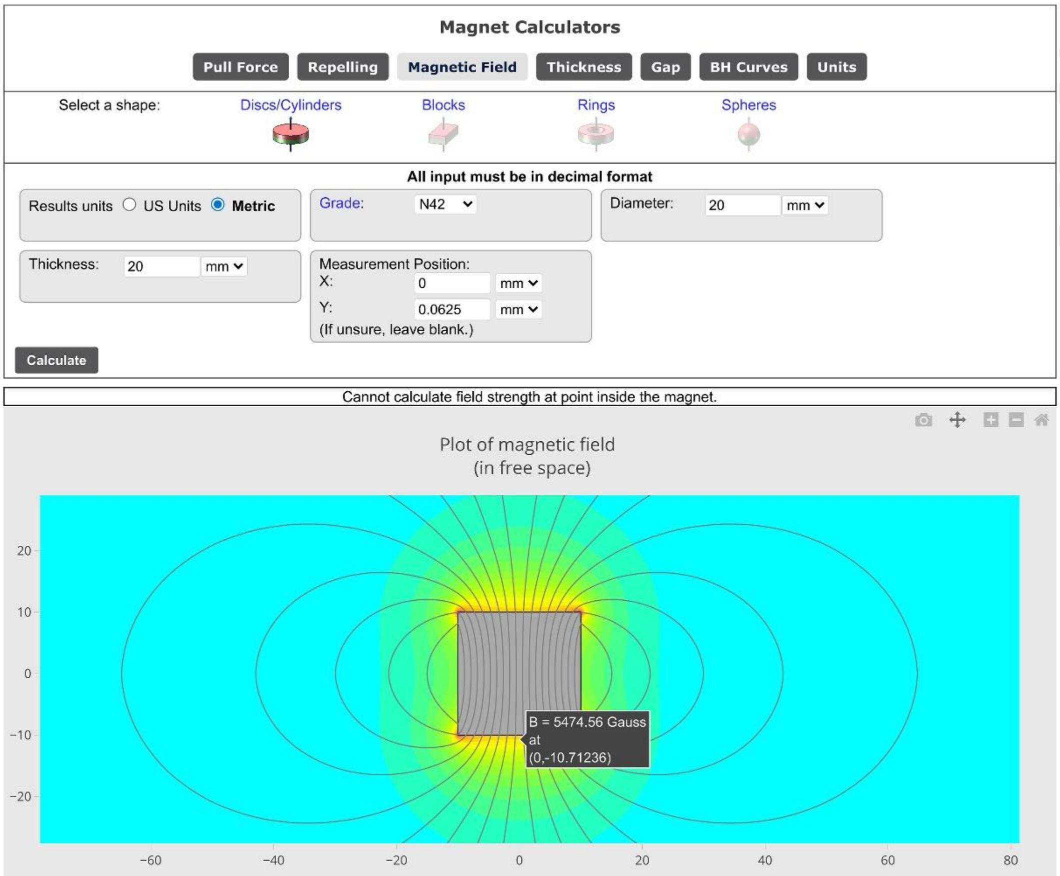

Figure 2. Calculating the magnetic field of NdFeB grade N42

Table 3. Specifications of the selected Neodymium magnet

Property	Value
Axial Length (L)	20 mm
Outer Diameter (D)	20 mm
Material Grade	NdFeB N42
Magnetic Flux Density (B)	5350 Gauss
Remanence (Br)	1.32 Tesla
Coercivity (Hc)	> 836 kA/m
Mass	47.51 gr

Maximum Operating Temperature	80 °C

3.2. Spring and Core Suspension

Another challenging part of the sensor was the design and fabrication of the internal suspension spring. The spring in the sensor plays a critical role in maintaining the precise axial position of the moving magnet and ensuring minimal eccentricity while retaining the sensitivity and stability of the sensor.

By investigating the available reference sample, the spring appeared made of a copper-based alloy, most likely a type of phosphor bronze or spring brass, based on its physical appearance, glint, elasticity, and non-magnetic behaviors. Spring design based on accurately determining of material and mechanical properties is essential to achieve proper sensor performance. However, the non-standard shape and design of the spring, significantly different from commercial helical or coil springs, posed significant challenges in determining its spring constant.

Accordingly, as illustrated in Figure 3, a wide range of spring prototypes with varying geometries were designed and fabricated using a precision laser cutting process. The spring constant of each prototype was then determined through experimental testing. Two metal alloys were selected for spring fabrication: Cu-Be (2%) and Cu-Zn (35%), with thicknesses of 0.1 mm and 0.2 mm, respectively.

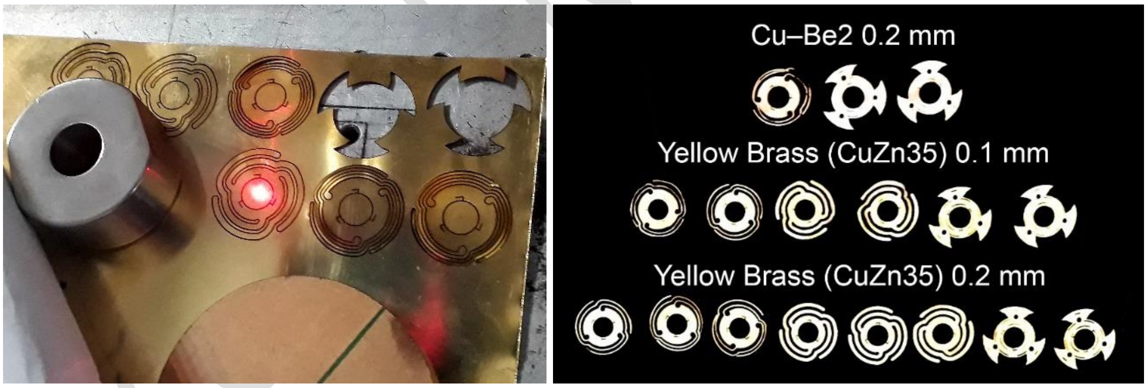

Figure 3. left) Spring production process using precision laser cutting; right) Fabricated springs with different materials and geometries

To accurately determine the spring stiffness, a custom-designed test stand was developed, that could precisely simulate the central alignment of the springs in the sensor assembly. The springs' flat arms are held horizontally on the sensor holder, similar to the installation configuration. After identifying the initial (zero) position of the spring prior to loading, standard weights were incrementally applied, and the resulting displacement from the zero position was precisely measured at each step.

It should be noted that the maximum possible stroke for the magnet is 4.5 mm in both up and down directions. Therefore, given the exact weight of the magnet (47.51 g), as well as the approximate weight of two symmetric metallic caps (6.84 g each) holding the magnet at both upper and lower sides, the minimum spring constant required to maintain the magnet in the center of the coil could be estimated. In Figure 4, the static displacement of the spring was plotted versus spring constant, which was calculated using Hooke's Law as different loads were applied.

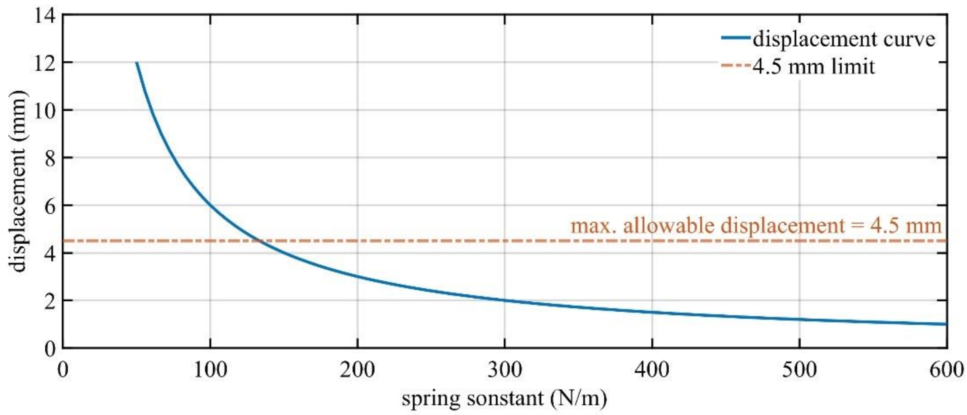

Figure 4. Displacement vs. spring constant by applying loads

It can be observed that springs with a stiffness of about 120 to 150 N/m fall within this range and are appropriate for the design. As examples, Figure 5 presents the stiffness measurements for two selected springs out of 32 prototypes, both made of Yellow Brass (Cu-Zn 35%) with thicknesses of 0.1 mm and 0.2 mm, and featuring two different geometries.

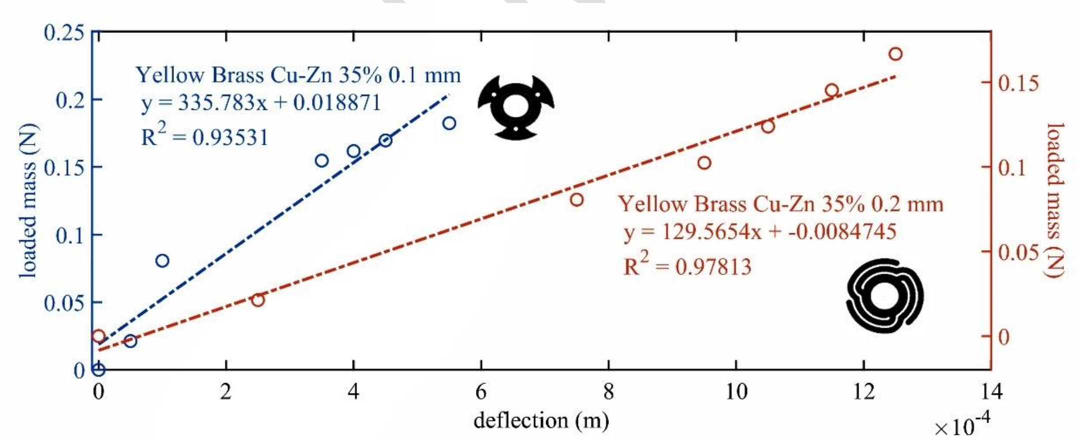

Figure 5. Measuring the springs' stiffness through experimental testing

The obtained results indicated that the spring made of Cu-Zn 35% with a thickness of 0.2 mm and the selected geometry provided a spring constant of 129.4654 N/m, which falls within the required range. This level of stiffness ensures that the magnet remains properly centered under normal operating conditions while allowing sufficient displacement to induce measurable voltages in response to vibrations applied at the sensor's base.

3.3. Inductive Sensing Core and Coil Parameters

According to the design requirements outlined in Table 2, generating the desired induced electromotive force (e.m.f.) based on the selected magnetic flux density necessitates a coil winding of approximately 8,000 to 15,000 turns, depending on the diameter of the wire used. Due to the limited space available for the coil and the need for many turns to meet design criteria, a 50 µm diameter wire was selected. Using Faraday's law and targeting a sensitivity of 10 mV/(mm/s), the required coil factor was determined, leading to an estimated value of 12,000 turns. This value was further refined by solving the governing electromagnetic equations in the Maplesoft™ environment, which confirmed that approximately 12,000 turns would be required to achieve the desired sensitivity. Additionally, based on the coil's geometry and material properties, the inductance value was estimated to be 5.5614 Wb/A.

In Figure 6, the final core component assembly of the signal generator including magnet, the magnet holder cap, flat springs, core body and wound coil are presented.

Figure 6. Assembled signal generator unit including magnet, springs, and coil

4- Experimental Test and Accuracy Verifications

In order to evaluate the performance of the sensor prototype, experimental tests were carried out. For this purpose, a rotating machine test stand was used to simulate the unbalanced fault. In Figure 7, the final prototype of the vibrometer sensor and test stand is presented. The test stand developed in the Intelligent Systems and Advanced Control Laboratory provides the capability to apply controlled unbalance conditions using standard masses at pre-defined radial distances [7, 25].

Two different data acquisition configurations were employed for distinct purposes. A low-rate sampling interval of 100 ms was used exclusively for trend analysis, and modeling of slow variations associated with inverter speed ramping, where high-frequency resolution was not required. These measurements were conducted over a 120 seconds interval, while the inverter frequency was incrementally increased at approximately 10 seconds steps. This dataset was used in accuracy verification and capturing the sensor's sensitivity.

In contrast, for frequency response analysis and dynamic characterization of the sensor, vibration signals were acquired using a high-resolution sampling frequency of 10 kHz (corresponding to a time step of 0.1 ms), which fully satisfies the Nyquist criterion for the investigated frequency range up to 1200 Hz. In this configuration, the sensor responses were recorded at rotational frequencies of 600, 1200, 1800, 2400, and 3000 rpm, with each operating condition maintained for 5 seconds to ensure steady-state behavior and reliable spectral estimation. This dataset was used for capturing the frequency response characteristics of the sensor.

4.1. Accuracy Verification

The objective of this test is to determine the sensitivity coefficient of the fabricated sensor. As previously stated, the sensor was designed to achieve a target sensitivity of 10 mV/mm/s. Given the precision of the machining process and the overall manufacturing quality, it is expected that this target sensitivity will be closely achieved.

Figure 8 shows the test conditions of the developed sensor to analyze the dynamic behavior of the sensor. For this purpose, a 150-gram unbalanced mass was placed at varying radii under different rotational speeds to amplify the vibration magnitude. This allows for continuous excitation of the sensor and increases the observability of its responses.

Figure 7. The final prototype of the vibrometer sensor (left); prepared test stand to conduct the experimental performance evaluation (right).

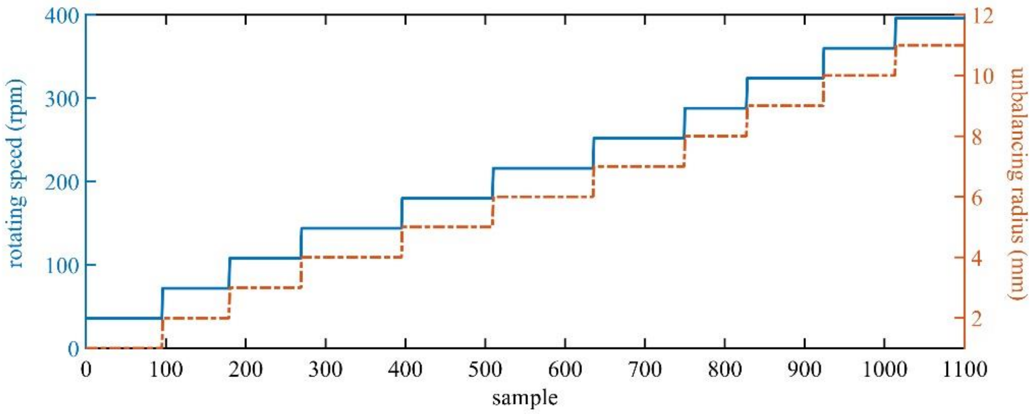

Figure 8. Test conditions for evaluating the dynamic response of the developed vibrometer sensor under unbalanced excitation.

The output voltage (e.m.f.) of the sensor output and the magnitude of vibration velocity at the motor base plate are measured simultaneously to obtain an accurate analysis of the sensor's behavior and to calculate the sensitivity slope. A precise and calibrated reference sensor was employed to measure the vibration velocity at the device's base. All measured data were recorded in real time for subsequent analysis. Figure 9-a shows the output voltage amplitude of the vibrometer under different operating conditions. Figure 9-b shows the amplitude of the vibration displacement and the corresponding vibration velocity measured by the reference sensor. Finally, Figure 9-c shows the relationship between the sensor output voltage (e.m.f.) and the measured vibration velocity.

Plotting the vibrometer's output voltage against the measured vibration velocity reveals a clear linear relationship, indicating consistent and predictable sensor behavior. This linearity allows direct calculation of the sensor sensitivity coefficient based on the slope of the e.m.f. vs. velocity curve. The resulting sensitivity for the developed sensor was approximately 9.4374 mV/mm/s, indicating a consistent and predictable response across the tested range. This linear response is a significant advantage, enabling the sensor to be easily integrated into practical measurement systems. By designing a suitable transmitter circuit, this sensor can be effectively used for accurate and real-time monitoring of vibration velocity in industrial or research applications.

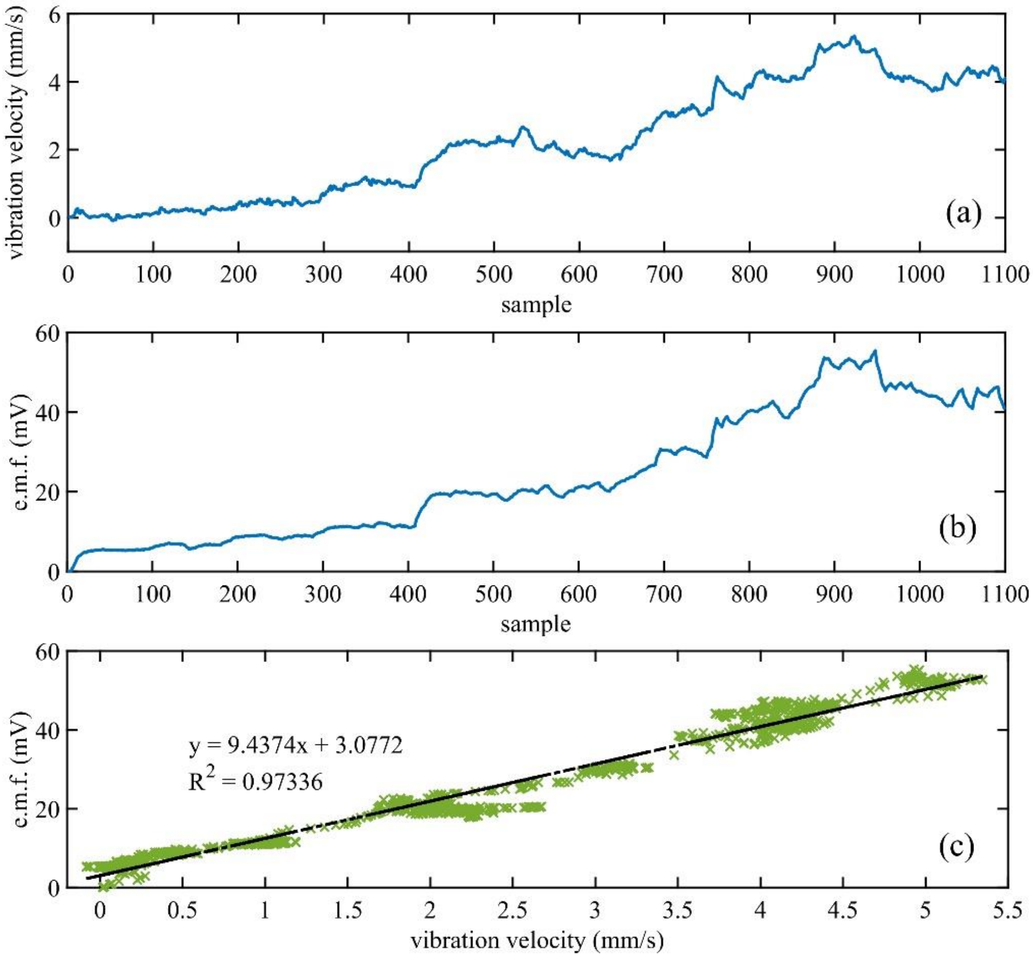

Figure 9. Sensor output and the magnitude of vibration velocity under varying vibration conditions: a) Displacement amplitude and corresponding vibration velocity measured by the reference sensor; b) Output voltage (e.m.f.); c) Correlation between e.m.f. and measured vibration velocity for sensitivity analysis.

4.2. Frequency Response Characteristics

Figure 10-a shows the vibration signal measured by the developed sensor on the test rig during an incremental increase in rotational speed. The vibration velocity amplitudes were calculated using the calibrated sensitivity slope obtained in Section 4.1 (k = 9.4374 mV/mm/s), where the measured output voltage was divided by the experimentally determined sensitivity of the sensor. The sensor responses were recorded at rotational speeds of 600, 1200, 1800, 2400, and 3000 rpm. At each speed level, the signal was recorded for 5 s to capture the steady-state response. In addition, at the maximum speed of 3000 rpm, the signal was continuously recorded for 30 s with a sampling interval of 0.1 ms to ensure sufficient temporal resolution for spectral analysis. Figure 10-b presents the corresponding frequency spectrum of the recorded signal after applying a Hanning windowing to reduce spectral leakage [26].

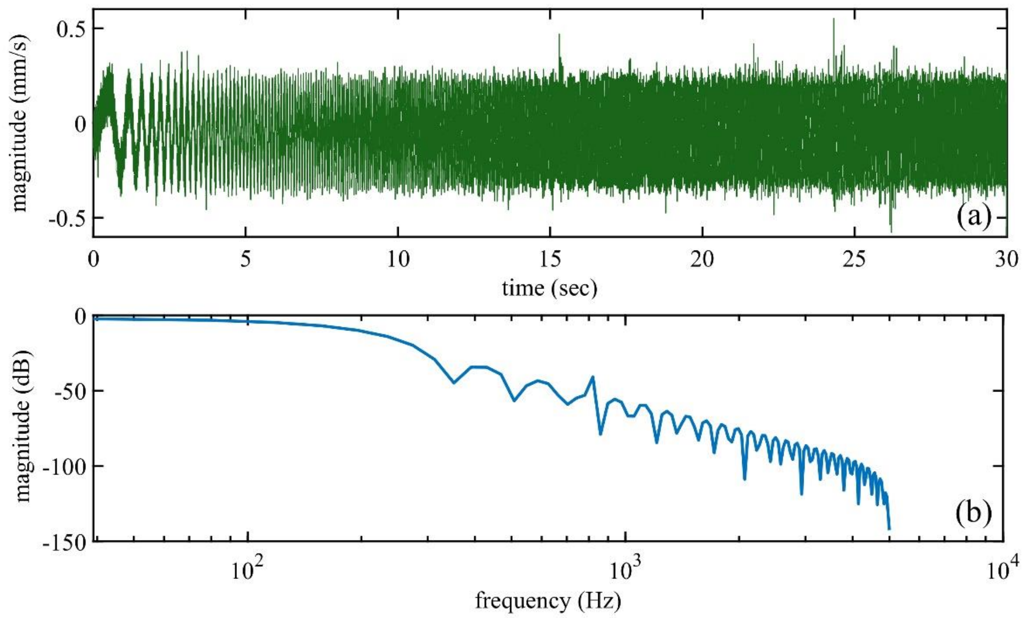

Figure 10. (a) Time-domain vibration signal of the developed velocity sensor (b) Frequency spectrum of the signal

The observed band-pass behavior is characteristic of a seismic velocity transducer, which can be modeled as a second-order mass-spring-damper system. This system consists of the effective mass of the moving permanent magnet ($m \approx 61$ g, including the end caps), the equivalent stiffness of the suspension springs ($k \approx 129$ N/m), and damping mechanisms that are mainly attributed to electromagnetic damping arising from the magnet-coil interaction and viscous air friction. Based on the oscillation spectrum obtained in Figure 10 and the expected behavior of such systems, the dynamic response of the sensor corresponds to a system close to critical damping ($\zeta \approx 1$), and therefore exhibits a band-pass filtering characteristic. The dynamic parameters of the system were identified through least-squares fitting between the analytical response and the experimental magnitude response.

Figure 11 shows the frequency response of the developed vibrometer sensor, where the horizontal axis is the frequency (in Hz) and the vertical axis is the magnitude of the response (in dB). The overall frequency response of the sensor clearly demonstrates bandpass filter behavior, characterized by a defined lower and upper cutoff frequency.

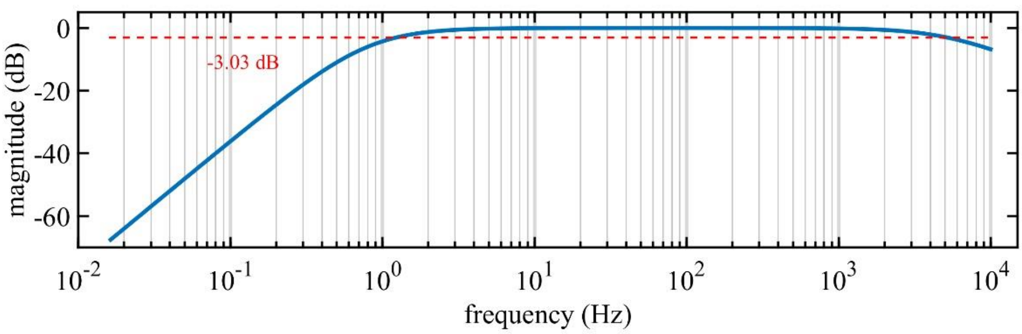

Figure 11. Frequency response magnitude of the developed vibrometer sensor

At both low and high frequencies, the signal amplitude is significantly attenuated, whereas in a specific intermediate frequency range, the sensor maintains a stable and flat response close to 0 dB. The defined frequency ranges along with the corresponding sensor behavior are summarized in Table 4.

Table 4. Sensor behavior across defined frequency bands

Operating Range	Frequency Range	Sensor Behavior
Lower cut-off frequency	f < 1.225 Hz	Severe signal attenuation (down to -60 dB)
Transition band	1.225 Hz < f < 10 Hz	Transition to pass-band
Operating frequency range	10 Hz < f < 1154 Hz	Pass-band around 0 dB
Transition band	1154 Hz < f < 5143 Hz	Transition to stop-band
Upper cut-off frequency	5143 Hz < f	Severe signal attenuation (down to -40 dB)

Given the band-pass nature of the sensor's frequency response, an appropriate transfer function can be developed to accurately model its dynamic behavior within the operational frequency range. This transfer function is essential for simulating the sensor behaviors, designing signal conditioning circuits, and integrating the sensor into wider measurement systems. Based on the measured frequency response and the pass-band characteristics, the transfer function can be represented as follows,

$$H(s) = \frac{K s^2}{\left(\frac{s^2}{\omega^2} + \frac{s}{q\omega} + 1\right)\left(\frac{s}{p} + 1\right)} = \frac{s^2}{3.108\times10^{-5} s^3 + s^2 + 10s + 25}$$

This formulation enables the sensor to be accurately represented in analog and digital signal processing environments, allowing for advanced analysis, filtering, and integration into vibration monitoring systems.

5- Discussion and Conclusion

In this paper, a single-coil vibrometer sensor was designed and fabricated to measure vibration velocity in high-inertia rotating machinery such as large steam and gas turbines. The design process involved selecting critical components, including a neodymium magnet, flat springs, a high-turn coil with 50 μm wire, and metal housings. One of the most challenging tasks was experimentally estimating the spring stiffness and material properties under geometric constraints. Since a direct, side-by-side experimental comparison between the developed sensor and a commercial velocity sensor was not feasible due to practical constraints, the design and validation of the proposed prototype were guided by the published specifications and expected performance characteristics of the commercial device. These included target sensitivity, linearity, effective bandwidth, and output voltage range.

As defined in the sensor design objectives, a sensitivity slope of 10 mV/(mm/s) was targeted; however, the fabricated prototype achieved a sensitivity of 9.4374 mV/(mm/s), corresponding to an approximate deviation of −5.626%. This deviation is primarily attributed to manufacturing and assembly tolerances. In particular, variations in the actual number of the coil's turns (on the order of ±5%), typical tolerances in magnet remanence and effective magnetic flux density for N42 NdFeB magnets (approximately ±3%), minor deviations in the air gap between the magnet and coil, and small centering inaccuracies of the flat suspension springs, where all influence the induced electromotive force. When these effects are combined, the resulting sensitivity reduction is consistent with the experimentally observed value and does not compromise the practical applicability of the proposed sensor. Despite slight deviations, the sensor showed very linear responses, which made it possible to compensate for deviations by using a properly calibrated transmitter in future implementations. The sensor's frequency response was also experimentally validated across the 3 to 1200 Hz range under low-amplitude excitations (0 ~ 4 mm) and peak vibration velocities up to 5 mm/s.

The novelty of this study lies in the precise fabrication methodology, mechanical tuning for low-frequency response, and thorough experimental validation rather than in the presentation of a new inductive sensing principle. Qualitative comparison indicates that the developed prototype exhibits comparable linearity and bandwidth behavior, supporting its suitability for practical low-frequency vibration monitoring applications. The final prototype provides a reliable output voltage proportional to the vibration velocity. Given the sensor's performance and its completely passive nature, requiring no external power supply, it can be used in power plants, oil, and gas facilities and similar environments to take advantage of its explosion-proof feature.

Future work will focus on developing an appropriate transmitter card, conducting tests in industrial environments, and enhancing the sensor's robustness for operation in harsh and noisy conditions.

Acknowledgment

This research was conducted with the financial support of the National Elite Foundation of Iran for problem-based student core projects, which is hereby acknowledged.

References

[1] S. Muthanandan and K. A. B. M. Nor, "Condition Monitoring and Assessment for Rotating Machinery," in *Rotating Machineries: Aspects of Operation and Maintenance*, S. A. Sulaiman Ed. Singapore: Springer Singapore, 2019, pp. 1-22.

[2] S. Amirkhani, A. Tootchi, and A. Chaibakhsh, "Fault detection and isolation of gas turbine using series–parallel NARX model," *ISA Trans.*, vol. 120, pp. 205-221, 2022/01/01/ 2022, doi: https://doi.org/10.1016/j.isatra.2021.03.019.

[3] R. B. Randall, *Vibration-based condition monitoring: industrial, automotive and aerospace applications*. John Wiley & Sons, 2021.

[4] A.-T. Watban Khalid Fahmi, K. Reza Kashyzadeh, and S. Ghorbani, "A comprehensive review on mechanical failures cause vibration in the gas turbine of combined cycle power plants," *Engineering Failure Analysis,* vol. 134, p. 106094, 2022/04/01/ 2022, doi: https://doi.org/10.1016/j.engfailanal.2022.106094.

[5] D. Neupane, M. R. Bouadjenek, R. Dazeley, and S. Aryal, "Data-driven machinery fault diagnosis: A comprehensive review," *Neurocomputing,* vol. 627, p. 129588, 2025/04/28/ 2025, doi: https://doi.org/10.1016/j.neucom.2025.129588.

[6] J. Li, C. Zheng, Z. Wu, H. Chen, X.-B. Wang, and Z.-X. Yang, "Review of fault diagnosis for rotating machinery: Prior knowledge integration in data-driven methods benefits model interpretability and generalizability," *Mechanical Systems and Signal Processing,* vol. 242, p. 113623, 2026/01/01/ 2026, doi: https://doi.org/10.1016/j.ymssp.2025.113623.

[7] R. Pedram and A. Chaibakhsh, "Multi-scale deep learning framework for robust bearing fault diagnosis in rotating machinery under sensor anomalies," *Journal of Control and Decision,* pp. 1-12, 2025/11/19 2025, doi: 10.1080/23307706.2025.2567006.

[8] M. Romanssini, P. C. C. de Aguirre, L. Compassi-Severo, and A. G. Girardi, "A review on vibration monitoring techniques for predictive maintenance of rotating machinery," *Eng,* vol. 4, no. 3, pp. 1797-1817, 2023.

[9] L. Ma, Z. Li, S. Yang, and J. Wang, "A Review on Vibration Sensor: Key Parameters, Fundamental Principles, and Recent Progress on Industrial Monitoring Applications," *Vibration*, vol. 8, no. 4, p. 56doi: 10.3390/vibration8040056.

[10] J. Duan, Z. Peng, L. Chen, and Y. Zeng, "A review of OMA parameter identification for hydro-turbine unit: Challenges in condition monitoring," *Renewable and Sustainable Energy Reviews,* vol. 217, p. 115724, 2025/07/01/ 2025, doi: https://doi.org/10.1016/j.rser.2025.115724.

[11] A. Hambaba, E. Huff, and U. Kaul, "Detection and diagnosis of changes in the time-scale eigenstructure for vibrating systems," in *2001 IEEE Aerospace Conference Proceedings (Cat. No.01TH8542)*, 10-17 March 2001 2001, vol. 7, pp. 7-3220 vol.7, doi: 10.1109/AERO.2001.931397.

[12] E. P. Carden and P. Fanning, "Vibration based condition monitoring: a review," *Structural health monitoring,* vol. 3, no. 4, pp. 355-377, 2004.

[13] C. Scheffer and P. Girdhar, *Practical machinery vibration analysis and predictive maintenance*. Elsevier, 2004.

[14] S. Tumanski, "Induction coil sensors—a review," *Measurement Science and Technology,* vol. 18, no. 3, p. R31, 2007/01/19 2007, doi: 10.1088/0957-0233/18/3/R01.

[15] J. Hagedorn, F. Blanc, and J. Fleischer, "Handbook of coil winding," *Springer Berlin Heidelberg,* 2018.

[16] X. Zhou, Y. Ruan, X. Mou, Y. Yuan, and Y. He, "A Design of Electromagnetic Velocity Sensor with High Sensitivity Based on Dual-Magnet Structure," *Sensors*, vol. 22, no. 18*,* doi: 10.3390/s22186925.

[17] Z. Yao, Y. Liu, M. Xing, and X. Liu, "Optimal Design of Dual-Magnetic Ring Structure with High Uniformity and Flux Density for Seismic Monitoring Sensor," *IEEE Sensors Journal,* pp. 1-1, 2025, doi: 10.1109/JSEN.2025.3570541.

[18] L. Hong, W. Wang, Z. Yao, Q. Gao, and Z. Han, "Improving the magnetic field homogeneity by varying magnetic field structure in a geophone," *Review of Scientific Instruments,* vol. 89, no. 1, 2018, doi: 10.1063/1.5005847.

[19] J. Hong *et al.*, "Dual-coil micro-impedance resonance oil contaminant detection sensor based on microfluidic chip," *Sensors and Actuators A: Physical,* vol. 345, p. 113754, 2022/10/01/ 2022, doi: https://doi.org/10.1016/j.sna.2022.113754.

[20] M. Mirzaei, P. Ripka, A. Chirtsov, and V. Grim, "Eddy current speed sensor with magnetic shielding," *Journal of Magnetism and Magnetic Materials,* vol. 502, p. 166568, 2020.

[21] S. Basu and A. K. Debnath, *Power plant instrumentation and control handbook: a guide to thermal power plants*. Academic Press, 2014.
[22] M. Kaltenbacher, *Numerical simulation of mechatronic sensors and actuators*. Springer, 2007.
[23] G. Selvolini and G. Marrazza, "Sensor principles and basic designs," in *Fundamentals of Sensor Technology*: Elsevier, 2023, pp. 17-43.
[24] K. J. M. calculator. https://www.kjmagnetics.com/magnet-strength-calculator.asp (accessed.
[25] N. Khoshnood, S. Amirkhani, A. Tootchi, and A. Chaibakhsh, "Detection and Isolation of Unbalanced and Bearing Faults in Rotary Machinery Using Artificial Intelligence," in *2020 28th Iranian Conference on Electrical Engineering (ICEE)*, 4-6 Aug. 2020 2020, pp. 1-6, doi: 10.1109/ICEE50131.2020.9261061.
[26] C. S. Lessard, "Window Functions and Spectral Leakage," in *Signal Processing of Random Physiological Signals*, C. S. Lessard Ed. Cham: Springer International Publishing, 2006, pp. 175-193.